J Mater Sci: Mater Med (2008) 19:2325–2333
DOI 10.1007/s10856-007-3328-7

Functionally graded bioactive glass coating on magnesia partially stabilized zirconia (Mg-PSZ) for enhanced biocompatibility

Mohamed N. Rahaman · Yadong Li · B. Sonny Bal · Wenhai Huang

Received: 26 September 2007 / Accepted: 19 November 2007 / Published online: 23 December 2007

Abstract The coating of magnesia partially stabilized zirconia (Mg-PSZ) with a bioactive glass was investigated for enhancing the bioactivity and bone-bonding ability of Mg-PSZ orthopedic implants. Individual coatings of three different bioactive glasses were prepared by depositing a concentrated suspension of the glass particles on Mg-PSZ substrates, followed by sintering at temperatures between 750 °C and 850 °C. Two silicate-based glass compositions (designated 13–93 and 6P68), and a borosilicate glass composition (H12) were investigated. The microstructure and adhesive strength of the coatings were characterized, and the in vitro bioactivity of the glasses was compared by measuring their conversion kinetics to hydroxyapatite in an aqueous phosphate solution at 37 °C. The 6P68 glass provided the highest adhesive strength (40 ± 2 MPa) but showed very limited bioactivity, whereas the H12 glass had lower adhesive strength (18 ± 2 MPa) but the highest bioactivity. A functionally graded coating, consisting of a 6P68 interfacial layer and an H12 surface layer, was developed to provide a coating with high adhesive strength coupled with rapid in vitro bioactivity.

M. N. Rahaman (✉) · Y. Li
Department of Materials Science and Engineering, University of Missouri, Rolla, MO 65409, USA
e-mail: rahaman@umr.edu

Y. Li
School of Materials Engineering, Soochow University, Suzhou 215021, China

B. S. Bal
Department of Orthopaedic Surgery, University of Missouri, Columbia, MO 65212, USA

W. Huang
Institute of Bioengineering and Information Technology Materials, Tongji University, Shanghai 200092, China

1 Introduction

Zirconia (ZrO_2)-based ceramics were introduced in the 1980s as bearing materials for total hip arthroplasty (THA) because of concerns about catastrophic failure of alumina (Al_2O_3) femoral heads in vivo [1, 2]. ZrO_2 stabilized in the tetragonal phase, typically with 3 mole percent (mol%) yttria (Y_2O_3), referred to as yttria-stabilized tetragonal zirconia polycrystals (Y-TZP), has flexural strength and fracture toughness values that are almost twice those for Al_2O_3 [1]. However, Y-TZP undergoes transformation and degradation during steam sterilization at autoclaving temperatures or when exposed to aqueous liquids at physiologic temperatures [3]. Following a high rate of failure in vivo, resulting from altered manufacturing parameters, Y-TZP femoral heads were withdrawn in 2001 from orthopaedic applications [4]. ZrO_2 partially stabilized with magnesia (MgO), typically ~8 mol% MgO, referred to as Mg-PSZ, has flexural strength and fracture toughness values which are inferior to those for well-fabricated Y-TZP prior to degradation. However, the strength and toughness are still superior to those of Al_2O_3 [1]. It has been reported that Mg-PSZ did not suffer from the strength degradation of Y-TZP during low-temperature aging [5]. Mg-PSZ femoral heads are still approved for articulating against polyethylene (PE) acetabular cups in THA. It is also being evaluated as the femoral bearing material for articulating against PE in total knee arthroplasty (TKA) [1].

Since Mg-PSZ is bioinert, its application as the femoral bearing in TKA requires the use of bone cement, made

primarily of poly(methyl methacrylate), PMMA, granules and methyl methacrylate monomer, for firm fixation of the implant to the surrounding tissue. A concern with cement fixation of periprosthetic skeletal implants is the potential for cement fragmentation and deterioration, leading to periprosthetic inflammation, progressive bone loss, and eventual implant loosening [6]. Therefore, the elimination of bone cement, while obtaining durable implant-bone bonding, is desirable.

Coatings of hydroxyapatite (HA), $Ca_{10}(PO_4)_6(OH)_2$, have been widely applied to Ti alloys (typically a Ti-6Al-4V alloy) used as the femoral stem in THA and the tibial component in TKA in an attempt to improve their bonding to bone [7, 8]. Bioactive glass coatings on orthopaedic implants, such as Al_2O_3 [9] and Ti alloys [10–14], have also been explored. A characteristic feature of bioactive glass is the time-dependent conversion of the surface to HA in an aqueous phosphate solution, such as a simulated body fluid, leading to a strong bond with hard and soft tissues [15]. Bosetti et al. [16] deposited coatings of two different bioactive glasses, designated AP40 and RKKP, on Y-TZP to impart bioactivity to the surface. The AP40 and RKKP glasses had compositions in the system SiO_2–β-$Ca_3(PO_4)_2$–CaO–Na_2O–K_2O–MgO–CaF_2, which were different from the bioactive glasses investigated in the present work. An apatite later was formed on the AP40 and RKKP glass surface after soaking the coated substrate for 30 days in a simulated body fluid. Kim et al. [17] deposited composite coatings of a CaO–Na_2O–P_2O_5 glass and HA particles on disks of Y-TZP to enhance its biocompatibility [17]. The adhesive strength of the composite coating was 35–40 MPa, which was 60–80% higher than the value ($\sim$22 MPa) for HA coatings.

The objective of this work was to prepare and characterize a bioactive glass coating on medical grade Mg-PSZ for enhanced biocompatibility. The requirements for the coating included strong interfacial bonding to the Mg-PSZ substrate and measurable in vitro bioactivity. Coatings of three different glass compositions, designated 6P68, 13–93, and H12, were used. The 6P68 and 13–93 glasses are silicate-based compositions [14, 18], whereas the H12 glass is a borate-based composition [12] (Table 1). Both 6P68 and H12 were developed primarily for applications as bioactive glass coatings on titanium-based alloys used in orthopedic surgery. The 13–93 glass has a composition based on the 45S5 bioactive glass composition [15]. A benefit of the 13–93 composition is its superior viscous flow sintering characteristics when compared to 45S5 glass, allowing more facile conversion of 13–93 particles into dense coatings or solids [19]. A rationale for choosing these three bioactive glasses was the close match in thermal expansion coefficient between the glass and the Mg-PSZ substrate. This is important for reducing thermal stresses in the coating when cooled to room temperature after deposition at higher temperature, thereby reducing the potential for cracking or delamination of the coating.

Table 1 Composition of glasses

Glass	Composition (wt%)							
	SiO_2	B_2O_3	Na_2O	K_2O	CaO	MgO	Al_2O_3	P_2O_5
H12	7.0	43.4	7.7		35.0	–	3.2	3.7
13–93	53.0	–	6.0	12.0	20.0	5.0	–	4.0
6P68	67.7	–	8.3	2.2	10.1	5.7	–	6.0

2 Materials and methods

2.1 Materials

The bioactive glasses used in the present work were designated 6P68, 13–93, and H12. Table 1 gives the nominal composition of each glass. The glasses were prepared by melting the required quantities of SiO_2 (Fused quartz; Particle Processing & Classifying Corp., Patterson, NJ), $CaCO_3$, Na_2CO_3, MgO, K_2O, Al_2O_3, $NaH_2PO_4.2H_2O$ and H_3BO_3 (Reagent grade; Fisher Scientific; St. Louis, MO) in a platinum/rhodium crucible in air for 2 h at 1,100 °C for H12, at 1,300 °C for 13–93, and at 1,500 °C for 6P68 glass. The melt was stirred twice and poured into steel molds to prepare rods or quenched between two steel plates to prepare sheets. The glass sheets were crushed in a hardened steel mortar and pestle to form particles, which were sieved through stainless steel sieves (50 and 100 mesh) to give particles with sizes of 150–300 μm and $<$150 μm for subsequent experiments.

The coefficient of thermal expansion (CTE) of each glass was measured in a dilatometer (Model 1600; Orton, Columbus, OH) using rods (1.0 cm in diameter $\times$ 2.54 cm long) heated at a rate of 3.0 °C/min to the softening temperature (T_d). The CTE was determined between 150 °C and 550 °C with an accuracy of $\pm$3%, and the T_d was determined to within $\pm$1 °C. The glass transition temperature, T_g, and crystallization temperature, T_x, were measured with an accuracy of $\pm$2 °C by differential thermal analysis, DTA (Model DTA7; Perkin Elmer, Eden Prairie, MN), using glass particles (45–150 μm) heated at a rate of 10 °C /min in N_2.

2.2 Preparation of bioactive glass coatings

Suspensions of bioactive glass particles for use in coatings were prepared using two different particle sizes: $<$32 μm and $<$4 μm. Particles of size $<$32 μm were obtained by

grinding particles (<150 μm) in an agate mortar and pestle, followed by sieving through a stainless steel sieve (450 mesh), whereas particles of size <4 μm were obtained by wet ball milling particles (<32 μm) for 72 h in a polyethylene container, using ZrO_2 balls as milling media and 2-propanol as solvent. Suspensions were prepared by dispersing the particles (~30 vol%) in deionized water, using ammonium polymethacrylate (Davan C; molecular weight = 10,000–16,000; R. T. Vanderbilt Co., Norwalk, CT) as a dispersant (0.5 wt%) and Aquazol 500 (Polymer Chemistry Innovations, Tucson, AZ) as a binder (1 wt%). Coatings were deposited on substrates (2.5 cm × 2.5 cm × 1 mm) of medical grade MgO partially stabilized ZrO_2 (Mg-PSZ), kindly supplied by Signal Medical Corp., Marysville, MI, by dropping the slurry on the substrate and pulling a blade at a fixed height (~300 μm) over the substrate. After drying for 12 h at room temperature, the coatings were heated for 1–2 h at 500–600 °C (heating rate = 2 °C/min) to burn out the binder, and then sintered for 10–20 min at 750–850 °C (heating rate = 5 °C/min) to densify the coating. The specific sintering temperature used was dependent on the glass composition. Graded coatings consisting of two glasses were prepared using the same method, by depositing and densifying the first coating, followed by the second coating.

2.3 Characterizations of glass coatings

X-ray diffraction XRD (XDS 2000; Scintag, Cupertino, CA) was used to detect the presence of crystalline phases in the fabricated coatings. XRD was performed on the coated substrate using Cu K_α radiation ($\lambda = 0.15406$ nm) in a step-scan mode (0.05° per step; 2 s per step) in the range of 10–80° 2θ. The microstructure of the coatings and the interfacial region between the coating and the Mg-PSZ substrate was observed using scanning electron microscopy, SEM (S-4700; Hitachi, Tokyo, Japan).

2.4 Adhesive strength testing

The adhesive strength of each glass coating on the Mg-PSZ substrate was measured using an adhesion testing apparatus (Romulus universal test equipment; Quad Group Inc., Spokane, WA). An aluminum rod (2.6 mm in diameter), one face pre-coated by the manufacturer with an adhesive capable of withstanding a maximum stress of 70–100 MPa, was bonded to the coating by curing for 1 h at 150 °C. The system was mounted in the testing apparatus and the rod was pulled at a rate of ~2 mm/min until the coating failed. The adhesive strength was determined from the maximum load recorded. At least five tests were performed for each coating. After the adhesive strength test, the failure surface of the specimen was examined using SEM.

2.5 In vitro evaluation of bioactivity

The bioactivity of each glass was evaluated in vitro by determining the rate at which the glass converted to a calcium phosphate material (typically hydroxyapatite, HA) when placed in an aqueous phosphate solution. The formation of a calcium phosphate material in vitro is indicative of the material's bioactive potential in vivo [15, 20, 21]. During the conversion, the glass suffered a weight loss, and there was a change in the pH of the solution. These changes were used to monitor the kinetics of HA formation. The method for measuring the weight loss and the pH as a function of time is described in detail elsewhere [22, 23]. Briefly, 1 g of glass particles (150–300 μm) was placed in 100 cm^3 of 0.25 M K_2HPO_4 solution with a starting pH of 7.0 at 37 ± 2 °C. Weight loss measurements were made after removing the particles from the solution, washing the particles three times with deionized water, and drying for more than 12 h at 90 °C. The mass of particles was measured to an accuracy of ±0.01 g. After the glass particles were removed from the solution for the weight loss measurement, the solution was cooled to room temperature, and its pH was measured to an accuracy of ±0.1 (Accumet-AR25; Fisher Scientific, St. Louis, MO).

The structure and composition of the reacted layer on the glass particles were characterized by XRD and SEM, using the procedures described earlier. Compositional analysis of the reacted layer was also performed using energy-dispersive X-ray analysis in the SEM and Fourier transform infrared (FTIR) spectroscopy (Model 1760-X; Perkin Elmer, Eden Prairie, MN). FTIR and attenuated total reflectance FTIR (ATR-FTIR) were performed in the wavenumber range of 400–4,000 cm^{-1} on disks prepared from a mixture of 2 mg of the reacted glass particles and 150 mg of high-purity KBr.

3 Results and discussion

3.1 Thermal characteristics of glasses

The linear expansion of H12, 6P68, and 13–93 glass as a function of temperature is shown in Figure 1. For comparison, the linear expansion of the Mg-PSZ substrate measured under the same conditions is also shown. The coefficient of thermal expansion (CTE) determined for each material in the range 150–550 °C is given in Table 2. Based on the CTE values, on cooling the coated substrate

from the fabrication temperature (750–850 °C) to room temperature, a coating of H12 or 13–93 should experience a tensile stress in the plane of the substrate, whereas a 6P68 coating should experience a compressive stress. Practically, it is difficult to match the CTE values of the coating and the substrate. The development of a small compression in a glass coating is often preferred over a tensile stress because the tendency for developing cracks in the coating is reduced [24]. The softening temperatures (T_d) of H12, 6P68, and 13–93 glass are indicated in Fig. 1 and summarized in Table 2. They varied from 607 °C for borosilicate H12 glass, to ~651 °C for silicate 13–93 glass, and to 653 °C for silicate 6P68 glass.

The DTA data (Fig. 2) were used to determine a suitable range of sintering temperatures for each glass. The objective was to sinter the glass to as high a density as possible without causing crystallization. Typically, the sintering temperature should be between the glass transition temperature (T_g) and the crystallization temperature (T_x). The DTA pattern for H12 glass showed that $T_g \approx 575$ °C and a single crystallization peak with $T_x \approx 770$ °C, indicating a reasonably wide temperature range for sintering to be achieved. In the case of 6P68 glass, $T_g \approx 630$ °C and there appeared to be two crystallization events, with peak temperatures $T_{x1} \approx 785$ °C, and $T_{x2} \approx 915$ °C. The DTA data for 13–93 glass showed that $T_g \approx 606$ °C, and there appeared to be two crystallization events for this glass also, with $T_{x1} \approx 752$ °C, and $T_{x2} \approx 910$ °C. Following a few preliminary experiments, it was found that sintering for 10–20 min at 750 °C for H12 and 13–93 glass, and at 850 °C 6P68 glass produced dense coatings without measurable crystallization.

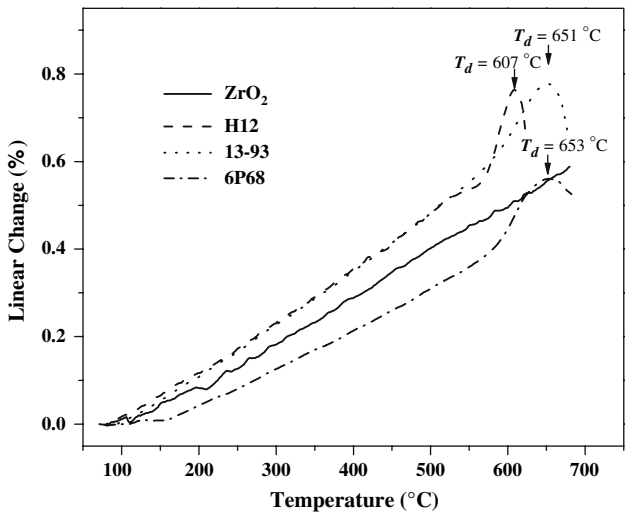

Fig. 1 Linear expansion as a function of temperature for H12, 6P68, 13–93 glass, and Mg-PSZ substrate

Table 2 Thermal properties of glasses and substrate (Mg-PSZ)

Material	α (10^{-6} °C^{-1})	T_d (°C)	T_g (°C)	T_{x1} (°C)	T_{x2} (°C)
H-12	12.3	607	575	770	
13–93	12.5	651	606	752	910
6P68	8.9	653	629	785	915
Mg-PSZ	10.6				

α = Coefficient of thermal expansion (measured between 150 °C and 550 °C)

T_d = Softening temperature

T_g = Glass transition temperature

T_x = Crystallization temperature(s)

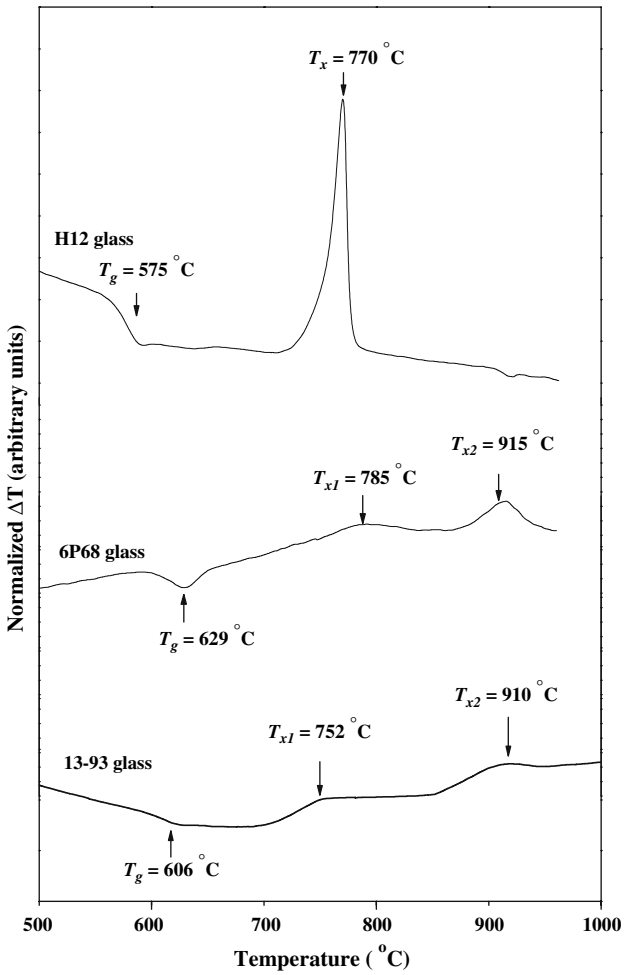

Fig. 2 DTA patterns for H12, 6P68, and 13–93 glass

3.2 In vitro bioactivity

Figure 3 shows the weight loss, ΔW, of the glass particles and the pH value of the solution as a function of time for H12, 6P68, and 13–93 glass particles (150–300 μm) reacted in 0.25 M K_2HPO_4 solution at 37 °C. The weight loss is defined here as $\Delta W = (W_o - W)/W_o$, where W_o is the

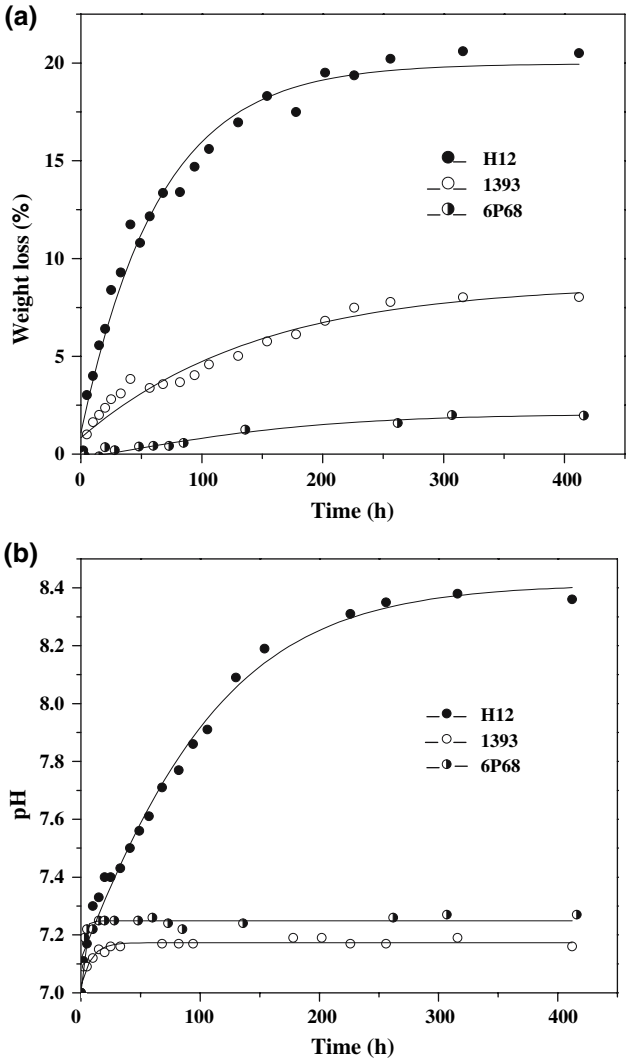

Fig. 3 (**a**) Fractional weight loss and (**b**) pH of the solution as a function of time for H12, 6P68, and 13–93 glass particles (150–300 μm) reacted in 0.25 M K_2HPO_4 solution at 37 °C

initial mass and W is the mass at time t. The ΔW value at any time was reproducible to ±2%. For H12 glass, ΔW increased rapidly with time and then reached a nearly steady limiting value of 20% after 200–300 h (Fig. 3a). In comparison, the ΔW for 6P68 glass showed a slow increase with time, reaching a value of 3% after 420 h when the experiment was stopped. The ΔW data for 13–93 glass increased faster than the data for 6P68, and reached a value of 8% after 420 h.

For 13–93 and 6P68, the pH of the solution (Fig. 3b) showed a small increase within 24 h, from 7.0 to ~7.2, but almost no further change at longer reaction times. On the other hand, for H12 glass, the pH increased more rapidly with time, reaching an almost steady value of ~8.3 after 200–300 h. In general, for H12 glass, the increase in pH with time showed approximately the same trend as the ΔW

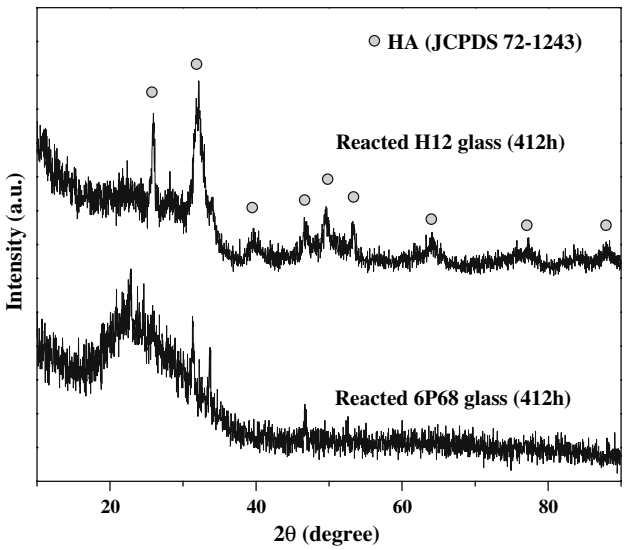

Fig. 4 XRD patterns for H12 and 6P68 glass particles (150–300 μm) after reaction for 412 h in 0.25 K_2HPO_4 solution at 37 °C

data. This is because the reactions that lead to the change in pH of the solution are the same reactions responsible for the weight loss [22, 23].

XRD patterns of the H12 glass particles (Fig. 4) after reaction for 412 h in the aqueous phosphate solution showed the presence of peaks that corresponded to those of a reference HA (JCPDS 72–1243). On the other hand, no clear evidence was found for the presence of HA in the reaction product of the 6P68 glass. The XRD data were in qualitative agreement with the weight loss and pH data which showed more rapid conversion of H12 glass in the phosphate solution.

The mechanisms of converting silicate and borate bioactive glass to a calcium phosphate material (typically hydroxyapatite, HA) have been discussed in detail elsewhere [15, 22, 23]. The rate of conversion to HA in an aqueous phosphate solution in vitro provides a measure of the bioactive potential of the material in vivo [15, 20, 21]. In the present work, the concentration of phosphate ions used in the solution (0.25 M) was far higher than that (0.001 M) in a simulated body fluid (SBF). This higher concentration was used to accelerate the rate of conversion to HA, in order to compare the relative rates of conversion to HA for the three glasses. Previous work showed that both H12 and 13–93 glass formed an HA layer on their surfaces when placed in an SBF for several days or more [12, 25]. On the other hand, 6P68 glass showed no ability to form an HA layer even after 30 days [14]. The inability of 6P68 glass to form an HA layer can be rationalized in terms of its high SiO_2 content (69 mol%) and, therefore, its high durability. Hench et al. [26] showed that for Na_2O–CaO–SiO_2 glass with high Na_2O and CaO content, and high $CaO:P_2O_5$ ratio, an SiO_2 content of <60 mol% was

required to achieve a reactive surface in an aqueous medium. The CaO content of 6P68 glass was lower than the values for H12 and 13–93, but this was not the limiting factor determining the ability to form and HA layer. Particles of lower durability Li_2O–CaO–B_2O_3 glass, having a lower CaO content than 6P68, have been observed to react completely in an aqueous phosphate solution to form HA [27].

3.3 Morphology and microstructure of coatings

Figure 5 shows SEM images of the cross-section of 6P68, H12, and 13–93 glass coatings on Mg-PSZ, prepared from suspensions of particles with a size of <4 μm. The thickness of the coatings was in the range 200–300 μm, and they appeared to be well bonded to the substrate. If required, thinner coatings can be prepared by other methods, such as dip coating in a suspension of glass particles, followed by sintering. The 6P68 and H12 coatings had a high density, but numerous fine pores and a few larger pores were present. The fine pores most likely resulted from gases trapped in the pores as the pores became isolated during the later stage of sintering. Sintering in a vacuum should lead to a reduction in the number of fine pores [28]. The few large pores were presumably caused by particle packing inhomogeneities in the coating [28]. Improvement in the colloidal stability of the suspension of glass particles, coupled with more homogeneous deposition of the coating, such as the use of dip coating, should alleviate the packing difficulties. The 13–93 glass coatings were more porous than the 6P68 and H12 coatings, developed an uneven surface after sintering, and were more prone to cracking. Because of these features, coatings of 13–93 glass were not used in subsequent experiments. For each glass, coatings prepared from particles of size <32 μm were more porous than coatings prepared from particles of size <4 μm. In subsequent work, coatings were prepared from particles of size <4 μm.

3.4 Adhesive bond strength

The measured bond strength for an H12 coating on Mg-PSZ was 18 ± 2 MPa, whereas for a 6P68 coating the bond strength was 40 ± 2 MPa. The values were determined as a mean and standard deviation from at least 5 measurements. SEM of the failure surface after the adhesive strength test indicated that failure occurred within the coating and within the epoxy (Fig. 6a, b). The occurrence of failure within the coating and the epoxy indicated that the adhesive bond strength of the 6P68 glass on Mg-PSZ was quite strong, greater than the value of ~40 MPa determined in the test.

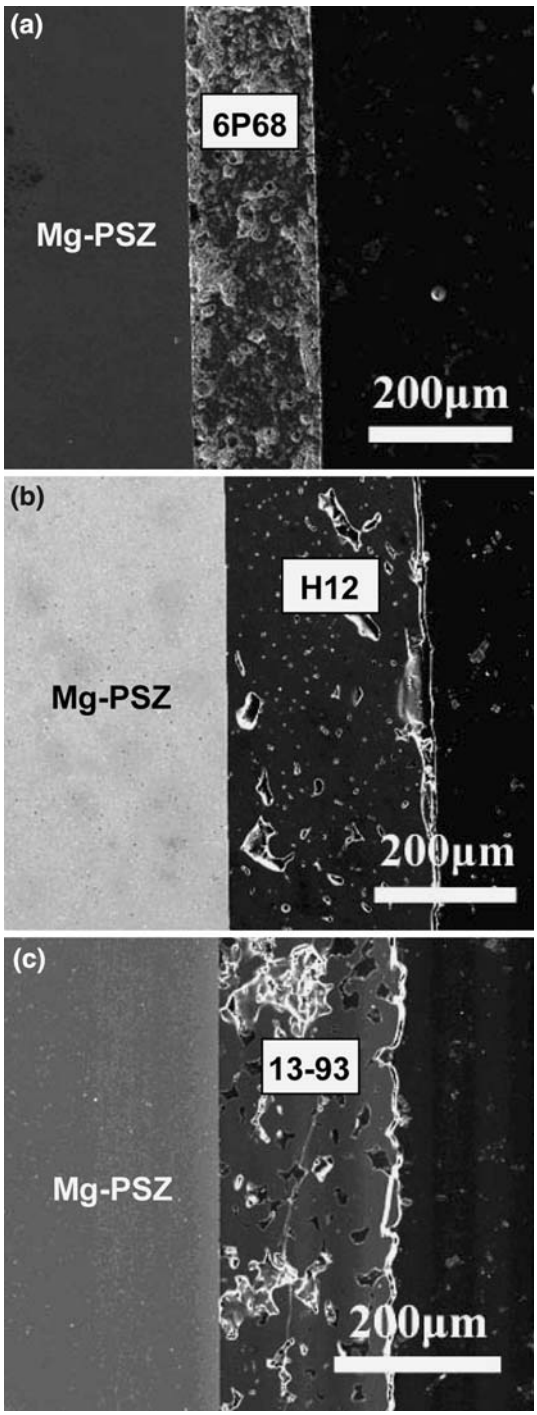

Fig. 5 SEM images of the cross-sections of glass coatings on Mg-PSZ substrates: (**a**) 6P68, (**b**) H12, and (**c**) 13–93

The cross-section view (Fig. 6c) showed that the coating adhered to the substrate after the adhesive strength test, with failure occurring within the coating. The failure mode of H12 coatings was similar to those for 6P68. The adhesive bond strength measured for 6P68 glass coatings on Mg-PSZ was comparable to the adhesive strengths (35–40 MPa)

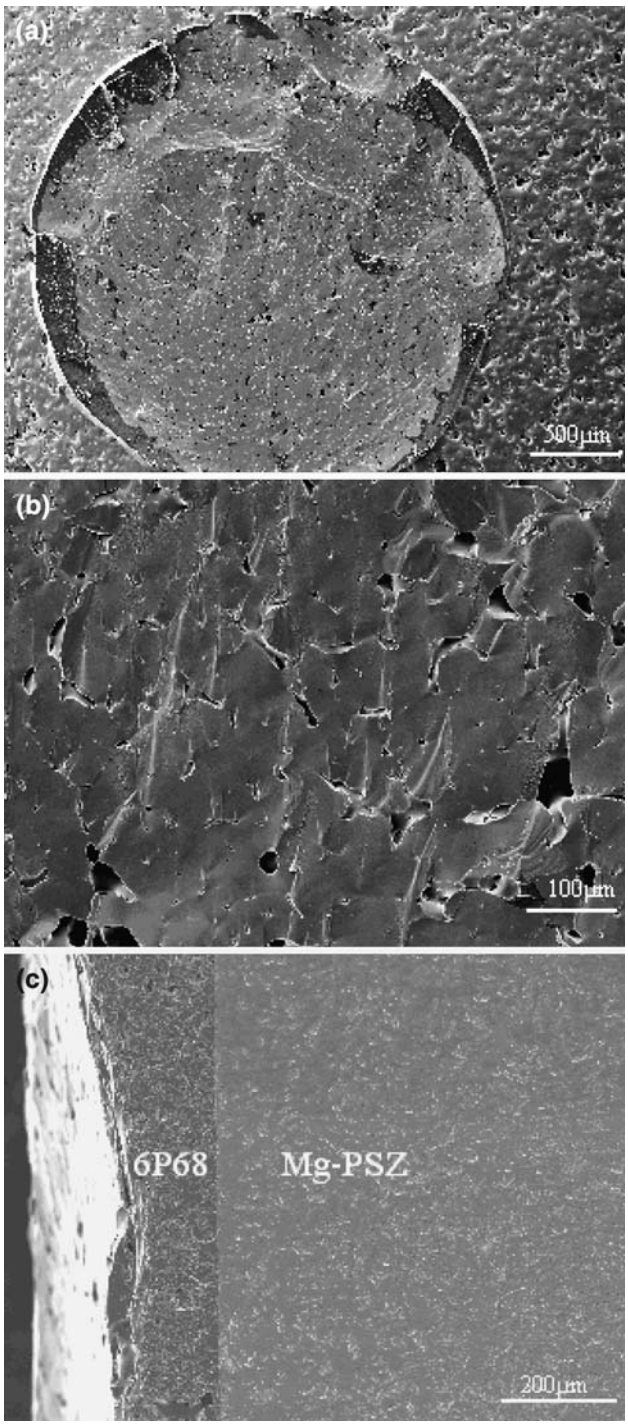

Fig. 6 SEM images of the failure region after adhesion strength testing of 6P68 glass coating on Mg-PSZ: (**a**), (**b**), surface region; (**c**) cross-section. Failure occurred in the coating but not at the interface with the Mg-PSZ substrate

measured by Kim et al. [17], using a similar test, for bioactive $CaO–Na_2O–P_2O_5$ glass coatings on Y-TZP substrates [17], and they were much higher than the adhesive strength (~22 MPa) for HA coatings on Y-TZP [17].

The test used in the present work was similar to that used by Kim et al. [17] to determine the adhesive strength of $CaO–Na_2O–P_2O_5$ glass coatings and HA coatings on Y-TZP substrates. In practice, the test suffers from a few drawbacks. The rod must be properly aligned with the surface of the plane of the coating to avoid peeling. Penetration of the adhesive into the coating can lead to weakening of the coating. In the present work, considerable care was taken to achieve optimum alignment. Several samples were prepared, and only those observed to have the best alignment were tested. It was unclear whether the adhesive penetrated into the glass coating. The 6P68 and H12 coatings had high enough density for the pores to be isolated, so penetration of the adhesive was only expected to occur into the surface pores.

3.5 Functionally graded bioactive glass coating

Based on the higher adhesive bond strength of the 6P68 glass coating, but its low reactivity in an aqueous phosphate solution, a multilayered approach was used to design a functionally graded coating. In this approach, 6P68 glass was used to form the first layer of a composite coating, providing strong bonding with the Mg-PSZ, whereas H12 was used to form the outer layer to provide bioactivity and rapid formation of HA on the coating surface. Figure 7 shows the cross-section of a composite coating of 6P68 and H12 on Mg-PSZ. The 6P68 layer appeared to be well bonded to the substrate. Both the 6P68 and H12 layers contained some porosity, but the interfacial region between the two glass layers was much denser. It appeared that interdiffusion between 6P68 and H12 produced enhanced sintering in the interfacial region between the two glass layers.

In vitro bioactivity of the graded composite layer was studied by placing the coated substrate in 0.25 M K_2HPO_4

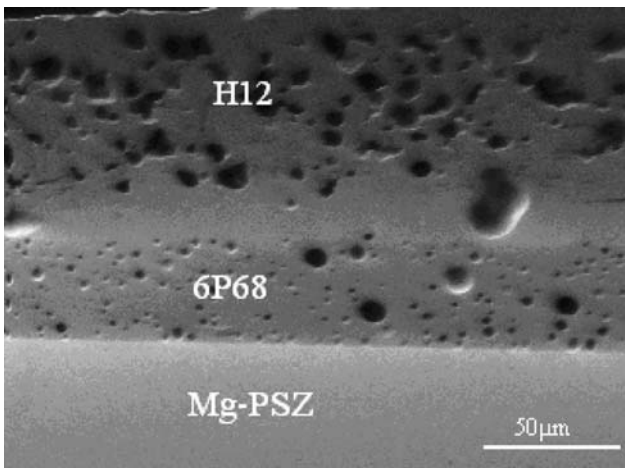

Fig. 7 SEM image of the cross-section of a graded coating of 6P68 and H12 glass on Mg-PSZ

solution at 37 °C and examining the coating surface for the formation of a calcium phosphate layer. Thin-film XRD analysis of the reacted surface (Fig. 8) showed the formation of HA (JCPDS 72–1243) within 5 h of reaction. The XRD pattern (5 h reaction) also showed small peaks corresponding to CaB_2O_4 (JCPDS 32–0155), presumably formed by a limited amount of crystallization of the H12 glass during sintering. The HA peaks became more intense after 1 day, presumably due to further conversion of the glass and thickening of the HA layer. The formation of HA on the glass surface was supported by FTIR reflectance spectroscopy (Fig. 9), which indicated the formation of a phosphate phase within 5 h, with the resonances becoming more intense after 1 day. The spectra showed the major

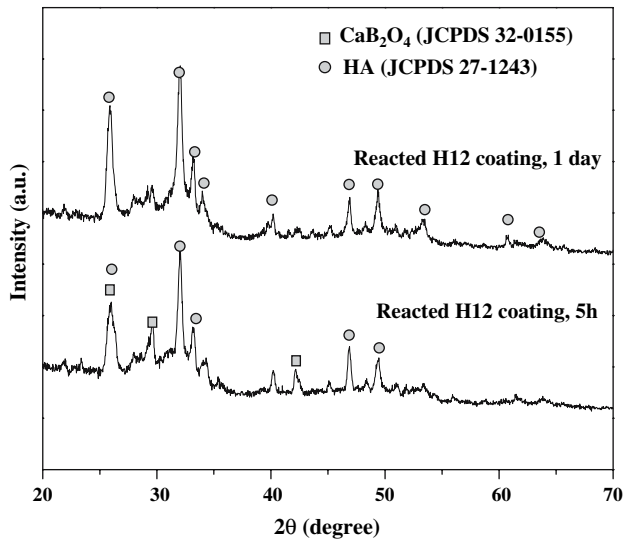

Fig. 8 Thin-film XRD patterns of the surface of a functionally graded coating (6P68 and H12 glass) on Mg-PSZ after immersion in 0.25 M K_2HPO_4 solution at 37 °C for 5 h and 1 day

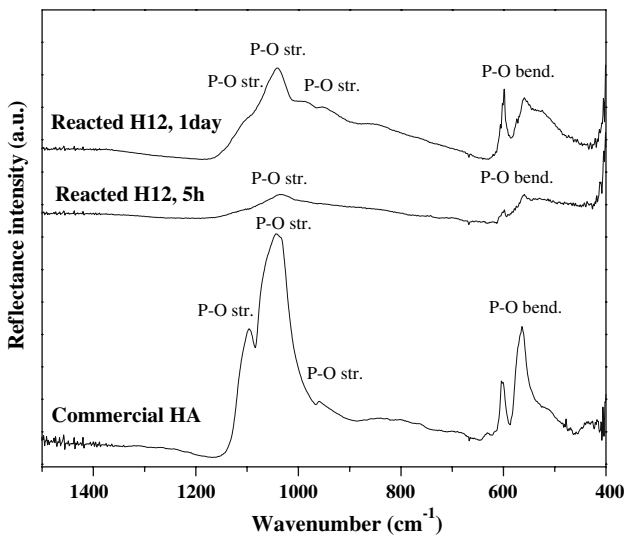

Fig. 9 FTIR reflectance spectra of a functionally graded coating (6P68 and H12 glass) on Mg-PSZ after immersion in 0.25 M K_2HPO_4 solution at 37 °C for 5 h and 1 day

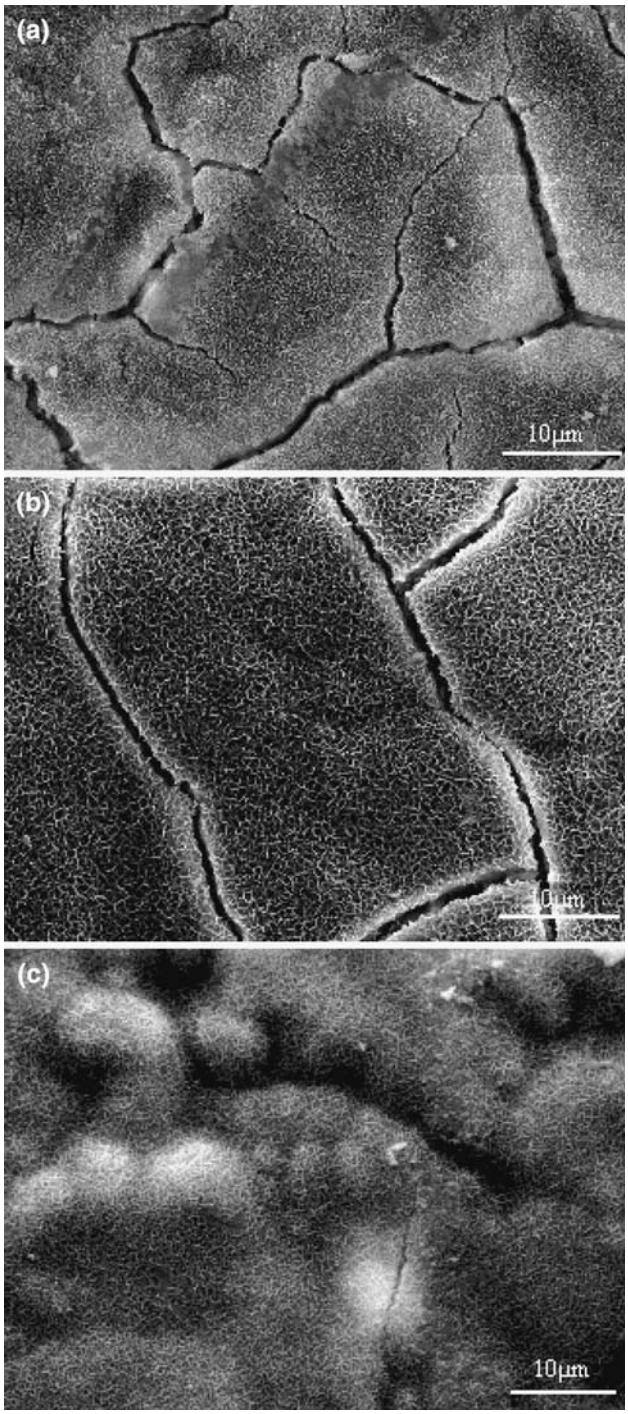

Fig. 10 SEM images of the surface of a functionally graded coating (6P68 and H12 glass) on Mg-PSZ after immersion in 0.25 M K_2HPO_4 solution at 37 °C for (**a**) 5 h, (**b**) 1 day, and (**c**) 15 days. Fine needle-like crystals, characteristic of hydroxyapatite, were formed on the surface

resonances associated with phosphate phase, at wavenumbers of $\sim 600\ cm^{-1}$ characteristic of the P–O resonance (bending) in PO_4^{3-} and at wavenumbers of $\sim 1{,}023\ cm^{-1}$ characteristic of the P–O resonance (stretching) in PO_4^{3-}. SEM showed the formation of fine needle-like crystals, characteristic of HA, on the surface of the composite coating (Fig. 10). The cracks on the surface of the coating were presumably caused by capillary stress during drying of the coating. Drying stresses are absent in vivo, so cracking of the HA layer should not be a concern.

Using a multilayered approach, the present work indicated that a functionally graded coating, combining strong interfacial bonding with an Mg-PSZ substrate and excellent bioactivity of the coating surface, can be produced. The strong interfacial bonding is beneficial for preventing delamination of the coating. The rapid formation of HA on the coating surface is beneficial for rapid bonding with surrounding tissues, providing for rapid fixation when a coated Mg-PSZ device is implanted into the body. These advantages of the functionally graded bioactive glass coating are encouraging for the eventual elimination of bone cement used for fixation of Mg-PSZ orthopedic bearings.

4 Conclusion

A functionally graded bioactive glass coating was formed on MgO partially stabilized ZrO_2 (Mg-PSZ) substrate by depositing particulate layers from a suspension, followed by sintering at 750–850 °C. The coating consisted of a silicate 6P68 glass bonded to the Mg-PSZ and a surface layer of borosilicate H12 glass. The adhesive strength between the 6P68 coating and the Mg-PSZ substrate was >40 MPa. In vitro testing of the coated Mg-PSZ substrate in 0.25 M K_2HPO_4 solution showed that a hydroxyapatite layer was formed within 5 h on the H12 surface layer. The strong bonding to the Mg-PSZ substrate coupled with the rapid in vitro bioactivity of the coating indicates the potential of the approach for promoting the fixation of Mg-PSZ implants to bone without the use of bone cement.

Acknowledgement The authors would like to thank Signal Medical Corp., Marysville, MI, for kindly providing substrates of medical grade Mg-PSZ.

References

1. M. N. RAHAMAN, B. S. BAL, J. P. GARINO, M. D. RIES and A. YAO, *J. Am. Ceram. Soc.* **90** (2007) 1965
2. C. PICONI and G. MACCAURO, *Biomaterials* **20** (1999) 1
3. J. CHEVALIER, L. GREMILLARD and S. DEVILLE, *Annu. Rev. Mater. Res.* **37** (2007) 1
4. J. L. MASONIS, R. B. BOURNE, M. D. RIES, R. W. MCCALDEN, A. SALEHI and D. C. KELMAN, *J. Arthroplasty*, **19** (2004) 898
5. G. FISCHMAN, N. BURLINGAME, B. UNGER, in "*Bioceramics:proceedings of the 6th International Conference on Ceramics in Medicine*", Edited by: P. DUCHEYNE and D. CHRISTIANSEN (Butterworth-Heinemann, Philadelphia, PA, 1993)
6. M. JASTY, W. JIRANEK and W. H. HARRIS, *Clin. Orthop. Rel. Res.* **285** (1992) 116
7. M. J. FILIAGGI, N. A. COOMBS and R. PILLIAR, *J. Biomed Mater Res.* **25** (1991) 1211
8. R. Y. WHITEHEAD, W. R. LACEFIELD and L. C. LUCAS, *J. Biomed Mater Res.* **27** (1993) 1501
9. L. L. HENCH and D. C. GREENSPAN, U.S. Patent 4,103,002, July 25, 1978
10. P. DUCHEYNE, *J. Biomed. Mater. Res.* **19** (1985) 273
11. G. GABBI, A. CACCHIOLI, B. LOCARDI and E. GUADAGNINO, *Biomaterials* **16** (1995) 515
12. L. PEDDI, M.S. Thesis, University of Missouri-Rolla, 2005
13. A. PAZO, E. SAIZ and A. P. TOMSIA, *Acta Mater.* **46** (1998) 2551
14. J. M. GOMEZ-VEGA, E. SAIZ and A. P. TOMSIA, *J. Biomed. Mater. Res.* **46** (1999) 549
15. L. L. HENCH, *J. Am. Ceram. Soc.* **81** (1998) 1705
16. M. BOSETTI, E. VERNE, M. FERRARIS, A. RAVAGLIOLI and M. CANNAS, *Biomaterials* **22** (2001) 987
17. H. W. KIM, G. GEORGE, J. C. KNOWLES, Y.-H. KOH and H.-E. KIM, *Biomaterials* **25** (2004) 4203
18. M. BRINK, T. TURUNEN, R.-P. HAPPONEN and A. YLI-URPO, *J. Biomed. Mater. Res.* **21** (1997) 114
19. M. N. RAHAMAN, R. F. BROWN, B. S. BAL, and D. E. DAY, *Semin Arthroplasty.* **17** (2006) 102
20. P. DUCHEYNE, *J. Biomed. Mater. Res.* **21** (1987) 219
21. T. KOKUBO and H. TAKADAMA, *Biomaterials.* **27** (2007) 2907
22. W. HUANG, D. E. DAY, K. KITTIRATANAPIBOON and M. N. RAHAMAN, *J. Mater. Sci. Mater. Med.* **17** (2006) 583
23. W. HUANG, M. N. RAHAMAN, D. E. DAY and Y. LI, *Phys. Chem. Glasses: Europ. J. Glass Sci. Technol. Part B* **47** (2006) 647
24. J. E. SHELBY, *Introduction to Glass Science and Technology* (The Royal Society of Chemistry, London, 2005)
25. Q. FU, M. N. RAHAMAN, B. S. BAL, W. HUANG, and D. E. DAY, *J. Biomed. Mater. Res.* **82A** (2007) 222
26. L. L. HENCH, R. J. SPLINTER, W. C. ALLEN, and T. K. GREENLEE Jr., *J. Biomed. Mater. Res.* **2** (1971) 117
27. K. P. FEARS, M. S. Thesis, University of Missouri-Rolla, 2001
28. M. N. RAHAMAN, *Sintering of Ceramics* (Taylor & Francis, Boca Raton, FL, 2007)